Boundary Layer Height and Entrainment Zone Thickness Measured by Lidars and Wind-Profiling Radars

STEPHEN A. COHN

Atmospheric Technology Division, National Center for Atmospheric Research, Boulder, Colorado

WAYNE M. ANGEVINE

Cooperative Institute for Research in Environmental Sciences, University of Colorado, and NOAA Aeronomy Laboratory, Boulder, Colorado

(Manuscript received 8 April 1999, in final form 24 September 1999)

ABSTRACT

The authors examine measurements of boundary layer height z_i and entrainment zone thickness observed with two lidars and with a radar wind profiler during the Flatland96 Lidars in Flat Terrain experiment. Lidar backscatter is proportional to aerosol content (and some molecular scatter) in the boundary layer, and wind profiler backscatter depends on the refractive index structure (moisture gradients and turbulence strength). Although these backscatter mechanisms are very different, good agreement is found in measurements of z_i at 1-h resolution. When the dataset is limited to daytime convective conditions (times between 1000 and 1700 LT), correlation coefficients between the profiler and each lidar are 0.87 and 0.95. Correlation between the two lidars is 0.99. Comparisons of entrainment zone thickness show less agreement, with correlation coefficients of about 0.6 between the profiler and lidars and 0.8 between the two lidars. The lidar measurements of z_i make use of coefficients of a Haar continuous wavelet transform of the backscatter profile. The wind profiler measurements use a standard technique. The wavelet transform technique is shown to provide consistent results with lidar data at 1-s time resolution.

1. Introduction

The daily cycle of convective boundary layer (CBL) growth and collapse is seen clearly in time–height displays of lidar backscatter intensity and in the reflectivity profiles of boundary layer (UHF) wind profilers. There are usually sharp gradients in aerosol concentration and specific humidity through the entrainment zone (EZ) at the CBL top as cleaner and dryer air from the free atmosphere is entrained and mixed into the aerosol-laden, moister boundary layer. The boundary layer height z_i often is taken as the middle of this EZ (the subscript i is due to the common use of a measured inversion height to define the CBL top). Growth of the CBL depends primarily on heat flux from the surface and stability characteristics of the free atmosphere above. Many CBL quantities scale with z_i, including gradients of mean wind speed, potential temperature and specific humidity ($\overline{U}$, $\overline{\theta}$, and $\overline{q}$); fluxes of momentum, potential temperature, and moisture; and variances (and higher-order moments) of vertical velocity. Stull (1988) discusses these scaling relationships and where they apply and provides a description of boundary layer (BL) evolution and definitions of z_i and the entrainment zone. The work described in this paper has two goals: to compare the z_i and EZ thickness (Δz_{ez}) measurements over many days from two ground-based lidars and a radar wind profiler and to evaluate an objective method to find the CBL height from lidar backscatter profiles using a continuous wavelet transform technique. We will refer to a measurement of z_i when averaging is done and to the CBL top when a nearly instantaneous measurement of the interface between boundary layer and free-atmosphere air is made.

Wind profilers are used commonly in boundary layer field campaigns to measure z_i. Results are shown in Angevine (1999) and Angevine et al. (1998a,b). Such measurements have been compared with radiosonde measurements by Angevine et al. (1994) and Grimsdell and Angevine (1998). Ground-based and airborne lidars are also used for z_i measurements (e.g., Piironen and Eloranta 1995). Eloranta and Forrest (1992) show correlations between lidar aerosol backscatter and moisture measured with an aircraft. This result leads us to believe we should find good correlation between lidar and wind profiler (whose backscatter is related to moisture gradients) z_i measurements. White et al. (1999) recently

Corresponding author address: Stephen A. Cohn, NCAR Atmospheric Technology Division, P.O. Box 3000, Boulder, CO 80307-3000.
E-mail: cohn@ucar.edu

presented comparisons of CBL height measured with a wind profiler and an airborne lidar over short time periods.

In convective boundary layers, aerosols and moisture often have sources at the surface, producing high concentrations in the mixed layer relative to the cleaner and drier free troposphere. These contrasts are the basis of lidar (aerosol) and radar wind profiler (moisture) measurements of z_i and EZ thickness. The entrainment zone consists of a mixture of air with mixed layer and free-troposphere characteristics. The EZ has been defined in various ways. In theory, it is the region in which the mean buoyancy flux is negative (e.g., Driedonks and Tennekes 1984). It effectively is impossible to measure flux profiles with sufficient precision to determine the EZ in real atmospheres with this definition. Another possible definition is the region in which the mean (over some space and/or time) virtual potential temperature, moisture, and/or aerosol profiles have strong gradients. This definition is workable for reasonably simple cases such as those to be discussed here, if mean profiles of those quantities on suitable scales are available. A third definition, particularly suited to remote sensing measurements and used in this work, is the region in which more than 5% but less than 100% of the air in a horizontal or temporal transect has free-troposphere characteristics such as low aerosol concentrations or low humidity (e.g., Boers et al. 1984; Crum and Stull 1987). In practice this definition is equivalent to finding the locations of percentiles (often nearer the center than 5% and 100%) of the CBL top. One difficulty with this definition is that not all fluctuations in the CBL top are associated with entrainment.

All these definitions imply that the entrainment zone thickness is an average property defined over a sizable distance, area, or time. Profiles from single rawinsonde ascents give only rough estimates of z_i and may be completely misleading for EZ depth, because the rawinsonde will find a very different result if it ascends in a thermal rather than between thermals (Stull 1988). Stationary ground-based remote sensors such as profilers and the lidars discussed here use temporal averaging rather than horizontal spatial averaging.

Measurements of Δz_{ez} are more rare and are hard to validate, and we believe the comparison of profiler and lidar Δz_{ez} presented here is unique. Boers and Eloranta (1986) present lidar measurements of the EZ using a scanning lidar and test a relation between Δz_{ez} and the measured jump in potential temperature at z_i. Davis et al. (1997) explored EZ measurements with an airborne lidar and found good correlation between two definitions based on the fluctuations in CBL height.

The wavelet technique for diagnosing z_i from lidar backscatter profiles is of interest because it can be used for automated recognition and applied to data with short integration times. This capability is valuable when examining small CBL features or analyzing data from a moving platform such as airborne lidar. A wavelet-based technique previously has been used by Davis et al. (1997) and Russell et al. (1998), but details of their implementations were not described. Davis et al. (2000) describe a more advanced wavelet implementation, and Steyn et al. (1999) present a parameterization technique with some similarity to wavelet-based techniques.

In this paper, we examine and present the evolution of the CBL top and EZ on several days during the Flatland96 Lidars in Flat Terrain (LIFT) experiment (Cohn et al. 1998; Angevine et al. 1998b). The Flatland96 LIFT dataset includes measurements by two lidars, a collocated boundary layer wind profiler, and a variety of supporting instruments. Section 2 describes the instruments and dataset used. Section 3 describes backscatter mechanisms for lidar and radar and introduces the wavelet transform–based measurement technique used to find the CBL top and z_i. Sections 4 and 5, respectively, present lidar and profiler comparisons of z_i and Δz_{ez}, and section 6 discusses limitations and complications of using the wavelet technique in CBL measurements.

2. Measurements from LIFT

The LIFT experiment brought together lidars and wind profilers to study the structure and evolution of the BL over the very flat terrain of central Illinois. LIFT took place within a larger companion experiment, Flatland96, during July and August of 1996.

We present measurements from two relatively new ground-based lidars and a nearby wind profiler. The lidars were within 4 m of each other, and the wind profiler antenna was about 20 m away. Because the wind profiler has a broad beam (a full width of 9° between the 3-dB points), its measurement volume included that of the lidars, beginning at about 270 m above ground level. The lidars are the high-resolution Doppler lidar (HRDL), which operates at a wavelength of 2 μm and is capable of providing profiles of backscatter and vertical velocity when staring and wind speed and direction when scanned (Grund 1996), and the staring/scanning aerosol backscatter lidar (SABL; Morley et al. 1996), which measures aerosol backscatter at two wavelengths (532 and 1064 nm). Both of these instruments recorded data with approximately 1-s time resolution during the experiment. HRDL has a range resolution of up to 30 m, and SABL can measure with 3.75-m resolution. The wind profiler is one of the common 915-MHz boundary layer profilers (e.g., Carter et al. 1995) and was part of a National Center for Atmospheric Research (NCAR) integrated sounding system (Parsons et al. 1994). The dates and times of availability of vertical data from each lidar are summarized in Table 1. Angevine et al. (1998b) give more information on the synoptic situation. Lidar data collection occurred in the daytime when an operator was present. The lidars were sometimes turned off during repairs, and HRDL operated part of the time as a scanning rather than vertically pointing lidar. The wind profiler operates unattended and provided nearly con-

TABLE 1. LIFT lidar vertical data (times are local time; Cu is cumulus).

Date	HRDL	SABL	Log entry
4 Aug 1996	1000–1700	1000–1700	Cu from 1020; afternoon cirrus
5 Aug 1996	1100–1700	1000–1700	Small Cu 1030; strong S wind at surface
6 Aug 1996	1000–1700	1000–1700	Cu onset at 1100
10 Aug 1996	1300–1700	None	Middle and high overcast, Cu
12 Aug 1996	None	1000–1700	Deep Cu, no precipitation light NNE winds
13 Aug 1996	None	1000–1600	Small Cu at 0940; clean air
14 Aug 1996	None	1400–1500	Clear; weak front pass early afternoon, no precipitation.
19 Aug 1996	1000–1700	1000–1700	Warm, S wind, scattered Cu all day
20 Aug 1996	1000–1600	1000–1700	Warm, clear, a few Cu towering in afternoon
21 Aug 1996	1000–1500	1100–1700	Warm, hazy, a few deep Cu in afternoon
22 Aug 1996	None	1000–1300	Warm, hazy

tinuous data. There were two other wind profilers within a few kilometers in addition to the collocated profiler. Wind profilers generally have 60-m range resolution, integrate for about 30 s, and vertical measurements are made every 2–3 min (oblique measurements are made in between vertical dwells). Supporting data were collected with ascents from a cross-chain loran atmospheric sounding system rawinsonde system, with cloud-base information from a commercial laser ceilometer, and with surface meteorological stations at the lidar site and nearby locations.

3. Backscatter profiles and a wavelet transform method

a. Lidar backscatter profiles

Backscattered power P_L from the SABL and HRDL lidars is given by the lidar equation,

$$P_L = \frac{\beta E \Omega \Upsilon A}{R^2} \frac{c}{2} \exp\left[-2 \int_0^R \alpha(R)\, d(R + 2\varepsilon R)\right], \quad (1)$$

where β is the backscatter coefficient of the atmospheric aerosols, E is the laser pulse energy, Ω is the overlap function between the transmitter and receiver, Υ is the optical transmission of the transmitter and receiver, A is the effective area of the receiver telescope, c is the speed of light, and R is the range to the backscatter volume. The range-dependent atmospheric absorption α and extinction ε coefficients are relatively small in a clean and cloudless atmosphere, and neglecting them only slightly changes the slope of the backscatter profile. In that case, the range-corrected backscattered power (also corrected for the range-dependent overlap function) is directly proportional to β, which, at the wavelengths of HRDL and the 1064-nm channel of SABL, is proportional to the aerosol concentration (number density). The 532-nm channel of SABL also has a significant range-dependent contribution from molecular backscatter, and this channel is not used in this work. In a well-mixed boundary layer, the aerosol concentration can be a tracer of BL air. Lidar backscatter profiles show generally high backscatter in the CBL, decreasing through the EZ, with weak backscatter in the free atmosphere. This gradient in backscatter is used to identify the EZ and local CBL top. Figures 1a,b show the daytime evolution of backscatter profiles from SABL and HRDL on 12 August 1996. The growth of the boundary layer is outlined clearly in both, with a decrease in intensity at the top of the CBL. The darkest regions are strong backscatter from clouds. Figure 1c shows the vertical velocity measured by HRDL. Notice the strong upward convective thermals feeding small cumulus clouds during the daytime and becoming weaker in the late afternoon.

b. Wind profiler backscatter profiles

The wind profiler backscattered power P_R is given by a similar equation, the radar equation,

$$P_R = P_T \frac{\eta G^2 \lambda^2 \theta^2 h}{1024 \pi^2 \ln 2 r^2}, \quad (2)$$

where η is the radar reflectivity per unit volume, P_T is the transmitted peak power, G is the antenna gain, λ is the radar wavelength, r is again the range to the backscatter volume, θ in this case is the beamwidth, and h is the pulse length and is twice the range resolution (e.g., Rogers and Yau 1996).

The wind profiler radar reflectivity is proportional to the refractive index structure constant C_n^2, which, in a turbulent boundary layer, is strongly dependent on gradients in q:

$$\eta = 0.38 C_n^2 \lambda^{-1/3}. \quad (3)$$

The average value of C_n^2 within the pulse volume is given by

$$C_n^2 = \frac{\langle [n(r + \delta) - n(r)]^2 \rangle}{|\delta|^{2/3}}, \quad (4)$$

where $\langle\ \rangle$ means a spatial average over the radar volume, δ is a spatial offset, and n is the radio refractive index, which is related to pressure P (kPa), temperature T (K), and q (g kg $^{-1}$) by

$$n = 1 + \left[\frac{776P}{T}\left(1 + \frac{7.73q}{T}\right)\right] \times 10^{-6}. \quad (5)$$

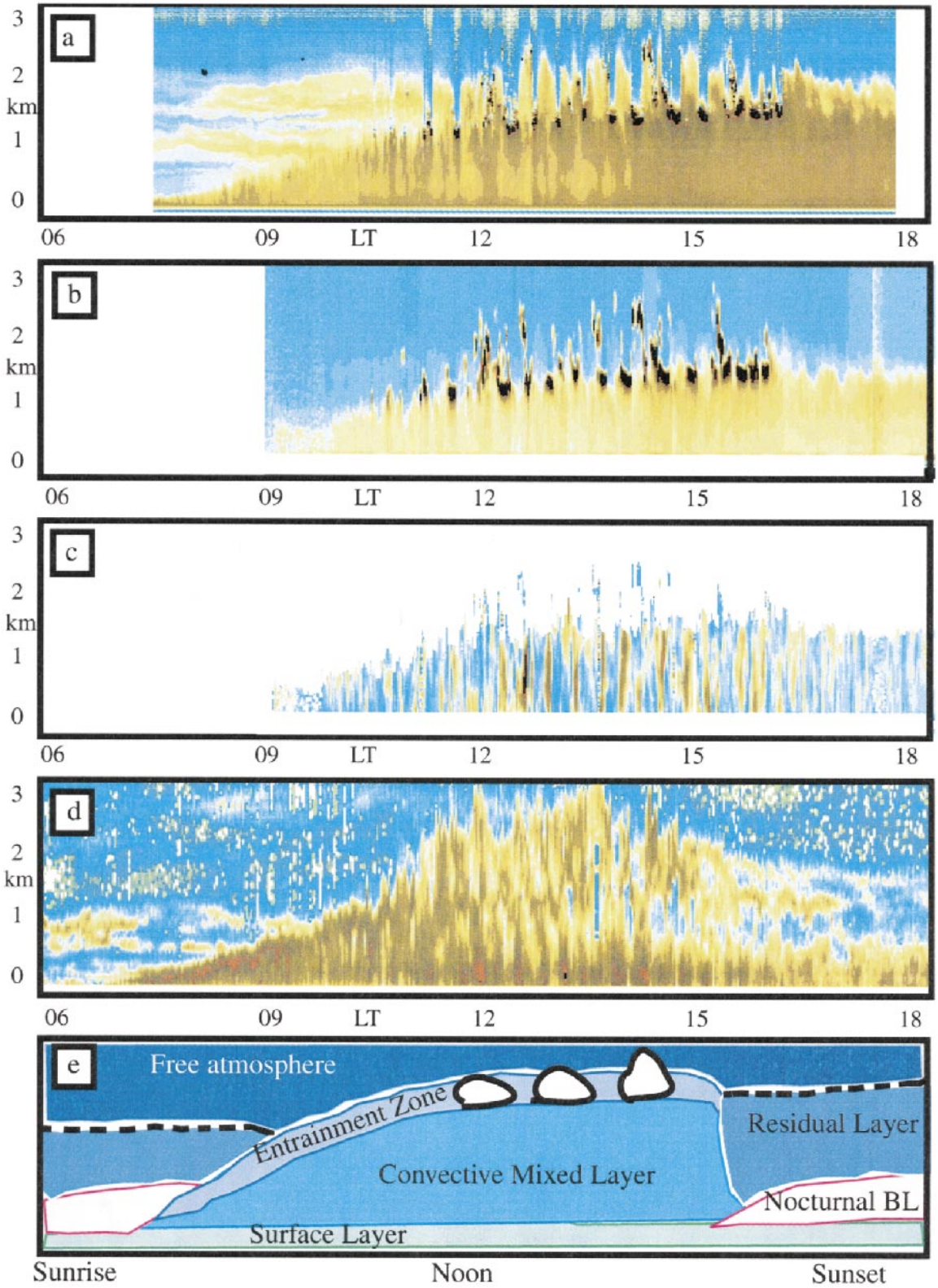

FIG. 1. A comparison of simultaneous observations of the boundary layer on 12 Aug 1996 at the LIFT Monticello site. (a) SABL backscatter, increasing in strength from blue to gold to black, (b) HRDL backscatter, and (c) HRDL vertical velocity. Brown and yellow represent updrafts that are often 1–3 m s^{-1}, with the strongest at 1300 LT being nearly 4 m s^{-1}, and velocities between -1 and 1 m s^{-1} are blue. The signal strength was insufficient to measure a velocity in the white space above. (d) Wind profiler backscatter, and (e) a sketch of typical boundary layer evolution (after Stull 1988).

In Eq. (4) the relevant δ is $\lambda/2$ because wind profilers see returns from Bragg scattering. We can see from these equations that large humidity gradients, along with the turbulent motions always present in the CBL, will cause large values of C_n^2 and therefore P_R. Because there is often a humidity gradient between CBL air and free-atmosphere air, we see a peak in wind profiler backscatter at the top of the CBL. This peak can be used to identify z_i, and, as will be discussed later, may be used to find Δz_{ez}. Figure 1d shows the growth of the CBL as seen with a wind profiler. The peak in reflectivity (red and dark-brown region) grows throughout the morning and becomes less well defined in the afternoon when more vigorous convection and clouds create many strong humidity gradients. Figure 1e schematically shows a day of convective boundary layer evolution [after Stull (1988)].

c. Use of wavelets

It is now clear that we can use a gradient locator to find the CBL top and z_i from lidar data and a peak locator to find it from wind profiler data. In clean data with a strong signature there are many simple algorithms that will do. For the lidar measurements, we have chosen to use wavelet coefficients because of the relative simplicity to implement a wavelet algorithm and the ability to use the wavelet transform to recognize the scale of the identified feature. The scale, represented by the wavelet dilation, can also be used for quality control, that is, to test the reasonableness of the algorithm result. The peak-locating algorithm used for the wind profiler data is that described in Angevine et al. (1994), although a wavelet could be used for this task also. This algorithm finds the peak in range-corrected signal-to-noise ratio (SNR) from an integration of approximately 30 s and composites these integrations (removing outliers) into a 1-h estimate of z_i.

The use of wavelet transforms in geophysical analysis has grown rapidly in recent years. Excellent books on wavelets and their applications include Foufoula-Georgiou and Kumar (1994), Chui (1992), and Walter (1994). Our application, after Davis et al. (1997), is a simple continuous wavelet transform (CWT) used for feature recognition and is not a full wavelet analysis or wavelet decomposition of the signal.

For a signal s and a wavelet Ψ, CWT for a position x and dilation D is given by

$$C_{P,D} = \frac{1}{D}\int_R s(t)\Psi\left(\frac{t-x}{D}\right)dt. \quad (6)$$

This equation is essentially a convolution, and, because $s(t)$ is a discrete (sampled in range) lidar or wind profiler signal, the integral is really a sum. Equation (6) is normalized by the dilation of the wavelet, which is consistent with Gamage and Hagelberg (1993) and Davis et al. (2000), though many definitions normalize by the square root of the dilation. Figure 2 demonstrates the CWT concept for a lidar backscatter profile. Figure 2a shows an idealized lidar backscatter profile (left) and the Haar wavelet (right), which is well suited to recognize a step function. Figure 2b shows a profile measured with HRDL and the two-dimensional array of Haar wavelet coefficients from this profile (refer to Fig. 8c for the wavelet coefficient array for an ideal profile). As in Eq. (6), a single wavelet coefficient is found by taking the inner product of the backscatter profile with the wavelet over the height region where both are defined. There are two degrees of freedom in this process, altitude and dilation. The wavelet inner product is applied many times as the wavelet center is translated over a range of heights, and the analysis is also repeated as the wavelet is stretched or ''dilated'' while retaining its shape. Because the Haar wavelet has equal area on either side of zero, the coefficient will be zero for a constant backscatter profile. In height regions where there is a sharp change in the profile, the coefficient will be large (positive if the profile decreases with height and negative if it increases). Efficient algorithms exist for computing CWT with commercial signal analysis software, or they can be computed directly. In the coefficient matrix of Fig. 2, the dark-blue border includes coefficients we have removed from our analysis. We have removed coefficients of the shortest dilations (usually less than 100 m), which come from compact variations in the height profile. These variations are often instrumental noise and sometimes are intensity variations within the CBL. We also have computed the CWT to dilations only as large as 1000 m. We found that the CBL top almost always is present as a strong feature within this range of coefficients. Longer dilations would require unnecessary computations and are more susceptible to errors from a varying backscatter profile above or below the CBL top (discussed further in section 6b). Last, we removed coefficients at dilations that are influenced by boundary effects. Boundary effects occur at altitudes that are less than one wavelet dilation from a boundary (the lowest or highest available data) where some terms of the convolution [Eq. (6)] are not defined.

For uncomplicated cases, using this subset of the CWT coefficients to find the CBL top is straightforward. We calculate the instantaneous CBL height from the altitude of the largest coefficient. In fact, this result would be quantized to the range resolution of the lidar, so, in practice, we have found it useful to use information in the neighborhood around the largest coefficient. Our algorithm does this by averaging two heights above and below and two dilations on either side of the largest value weighted by the coefficients. In this way we can estimate the instantaneous height to better than the range resolution of the instrument. The horizontal line of Fig. 2b is the algorithm result. We will discuss potential biases in automated calculation in section 6.

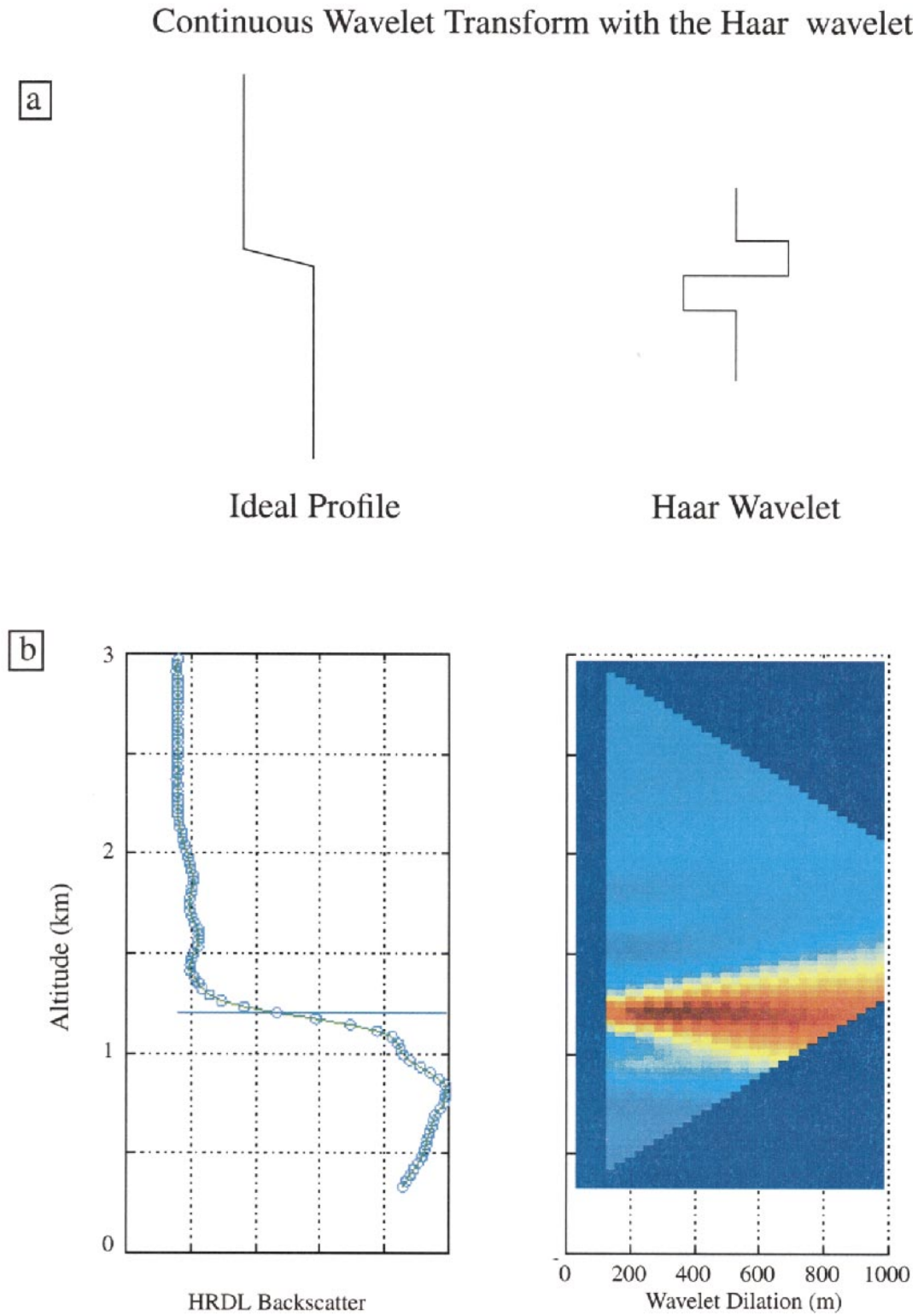

FIG. 2. (a) Idealized lidar backscatter profile, with uniform strong backscatter in the lower, well-mixed boundary layer, weak backscatter in the free atmosphere above, and (left) a transition through the entrainment zone; (right) the shape of the Haar wavelet. (b) A sample HRDL backscatter profile, (left) averaged to 10 min and (right) the corresponding wavelet transform coefficient matrix. The horizontal line corresponds to the altitude chosen as the local CBL top by the wavelet algorithm. The dark-blue background in the coefficient matrix is values we have masked out because of edge effects or the small scale of the features they represent. The coefficient magnitude increases as the color changes from blue through yellow to red.

4. Boundary layer height measurements

Figure 3a shows the CBL top calculated from 30-s averages (of the 1-s recorded data) during 2 h of HRDL backscatter measurements on 20 August 1996. The intensity is in arbitrary decibel units, and the CBL top appears as a very distinct gradient from brown to blue. Data below about 300 m are not valid, because the receiver is recovering from the transmit pulse. The algorithm finds BL height very well from these data, following slight rises and falls of the CBL top, probably as convective thermals advect past. This case is a very simple one, free of multiple layers of backscatter. We will discuss the effect of clouds, which appear as the very strong backscatter in red and black, later in section 6b.

Figure 3b shows a much higher resolution example from SABL, also on 20 August. This example is from 1-s measurements with SABL, and the plot covers 10 min. This figure shows fine details of the CBL top at many scales as the atmosphere advects over the lidar. There also are times when the CBL top is not so well defined. At 0920:30 LT, for example, the algorithm identifies a patch of ''dirty'' air that appears to be above the local CBL top. We believe the algorithm could be improved by incorporating continuity checks to identify possible outliers and by reporting a ''confidence'' in the result based on continuity and competing features in the wavelet coefficient map. The 1-s resolution in Fig. 3b represents about 5 m for a moderate wind speed of 5 m s^{-1} and would represent about 100 m if the data were taken from an airborne lidar. Davis et al. (2000) demonstrate a wavelet technique that achieves 0.2-s (20-m horizontal) resolution with an airborne system.

To compare measurements from the HRDL and SABL lidars and the wind profiler, we present Figs. 4 and 5. Figure 4 includes about 9 h of data on 6 August 1996 during which z_i was determined from the lidars and wind profiler with 1-h resolution by averaging 30-s CBL top measurements. The agreement is seen to be very good. Because SABL and HRDL are looking at nearly the same volume of atmosphere and use the same backscatter mechanism, it is expected that their results will be very close. In Fig. 5 we compare z_i calculated from pairs of sensors for the entire LIFT dataset, summarized in Table 1. This dataset includes all times between 1000 and 1700 LT when each pair of sensors had reliable data. Because there were many times the HRDL lidar was scanning rather than being vertically pointed and many times when each instrument was undergoing development, the number of points in each plot varies. Figure 5a compares profiler and HRDL 1-h results, with the expected 1:1 line overplotted. There is a high correlation coefficient for the entire experiment (0.95). Figures 5b,c show the same information, comparing the profiler and SABL, and HRDL and SABL. Again the correlations are high (0.87 and 0.99, respectively). Last, in Fig. 5d we compare 30-s measurements of CBL height from the two lidars, which have a correlation of 0.93. A slight bias in the lower z_i values, which are from the morning hours, can be seen in these plots, with HRDL apparently measuring a higher z_i than either the profiler or SABL. We believe this is a measurement bias produced by the interplay of the HRDL lidar focus distance and the effect of a sloped background on the wavelet algorithm. This possibility is discussed further in section 6b. We also see larger scatter between lidar and profiler at the higher z_i values. We attribute this scatter to the presence of clouds and the generally variable nature of the CBL top in convective conditions with strong updrafts. The overall agreement of these instruments is significant because of the different backscatter mechanisms of lidars and the wind profiler. Some of the agreement may be due to more than one of the instruments incorrectly identifying the top of a residual layer rather than the top of the CBL, however. We minimize this effect by limiting data analysis to daytime, convective periods and by carefully screening the results for this effect. Residual layers are discussed further in section 6c.

In Fig. 6 we present boundary layer height measurements with SABL with 30-s resolution on 13 August and 19 August 1996. The fluctuations in background intensity over time are instrumental. Unlike threshold techniques for CBL retrieval (e.g., Melfi et al. 1985), however, wavelet-based CBL retrieval is insensitive to these temporal fluctuations. On 13 August the CBL grows quickly to the height of an existing residual layer, and on 19 August the CBL grows more slowly throughout the day. On both days the algorithm is able to follow the growth of the CBL. The examples in Fig. 6 also illustrate the morning residual layer and the larger variance in 30-s CBL height estimates during afternoon convection and in the presence of clouds. Both of these features will be discussed further in section 6.

5. Entrainment zone thickness

As discussed in the introduction, a single backscatter profile or short time average of profiles contains little information about the entrainment zone thickness. The backscatter gradient may be sharp or broad depending on the history of the air in the field of view (e.g., recent mixing between CBL and tropospheric air would make the interface broad). When averaged over long times, during which a representative sampling of convective thermals and downdrafts pass over the instrument, the average backscatter profile would be expected to show Δz_{ez}. One would estimate a backscatter intensity in the free atmosphere and one in the BL and take the altitudes 5% and 100% along the transition between them. In practice, however, this method does not work well. Clouds during any part of the integration period will make it fail, because they will produce a very large return, and it is assumed that the backscatter is from only aerosols.

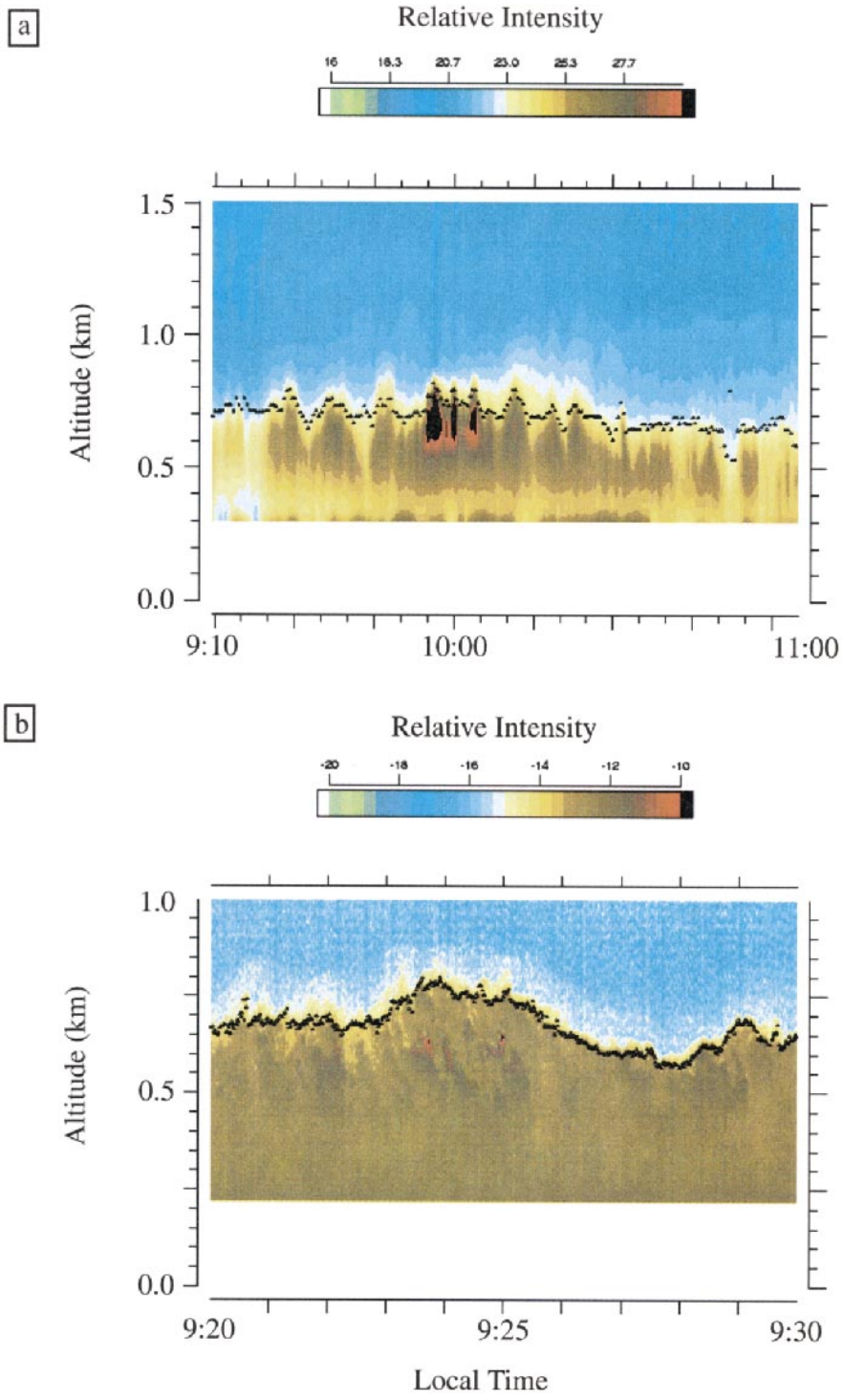

FIG. 3. (a) Local boundary layer height (triangles) computed from 30-s averages of HRDL backscatter overlaid on the backscatter profiles. These data are on the morning of 20 Aug 1996. (b) A similar computation but using SABL data and demonstrating 1-s measurements of local CBL top. Note differing horizontal and vertical scales.

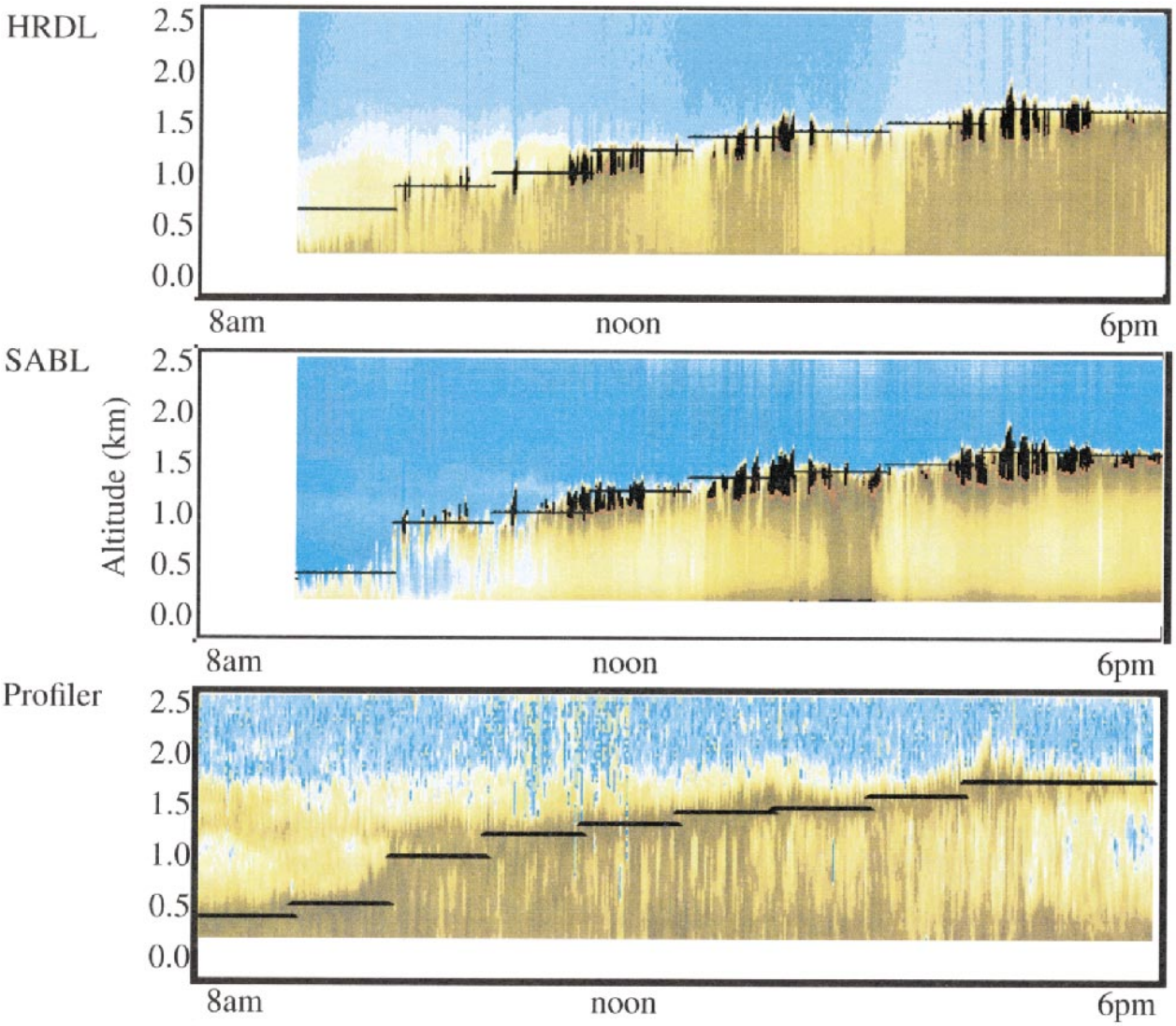

FIG. 4. A comparison of hourly z_i on 6 Aug 1996 from (top) HRDL computed with the wavelet transform algorithm on 30-s profiles, (middle) SABL using the same technique, and the wind profiler method of Angevine et al. (1994).

We have chosen an alternate way to calculate Δz_{ez}, based on variations of the CBL top over time. A time series of CBL top is measured from short time averages of backscatter, and from this time series a distribution of the interface height is found. The difference between appropriately chosen percentiles of the height of the interface gives Δz_{ez}. Percentiles are chosen to discount outliers of the distribution. The same algorithm has been used on wind profiler data (e.g., Angevine 1999), and Davis et al. (1997) describe a similar method for lidar data. Figure 7 shows results that compare Δz_{ez} measured in this way. In this case, the individual CBL-top measurements were at made 30-s intervals, and percentiles over each 1-h period were found. In addition, a linear trend was removed before the standard deviation was calculated, because the mean value of z_i changes throughout the day. To prevent outliers from influencing the result, we found the thickness from the distance between the 15th and 85th percentiles of the lidar data and the 25th and 75th percentiles for the wind profiler data. Each plot shows coincident measures of Δz_{ez} from a pair of instruments. As with the earlier comparison of z_i, we limited comparison times to between 1000 and 1700 LT. We also excluded thickness measurements greater than 800 m, which are likely to be false, or from times when the CBL top is not well defined. Last, we also excluded points at which the corresponding z_i measurements from the pair of instruments do not agree. Specifically, we excluded points at which the measured z_i differ by more than one standard deviation from the average difference. These average differences are listed in Fig. 7, as are the number of points remaining for the comparison. The 1:1 line and a best-fit line (forced through zero) also are shown.

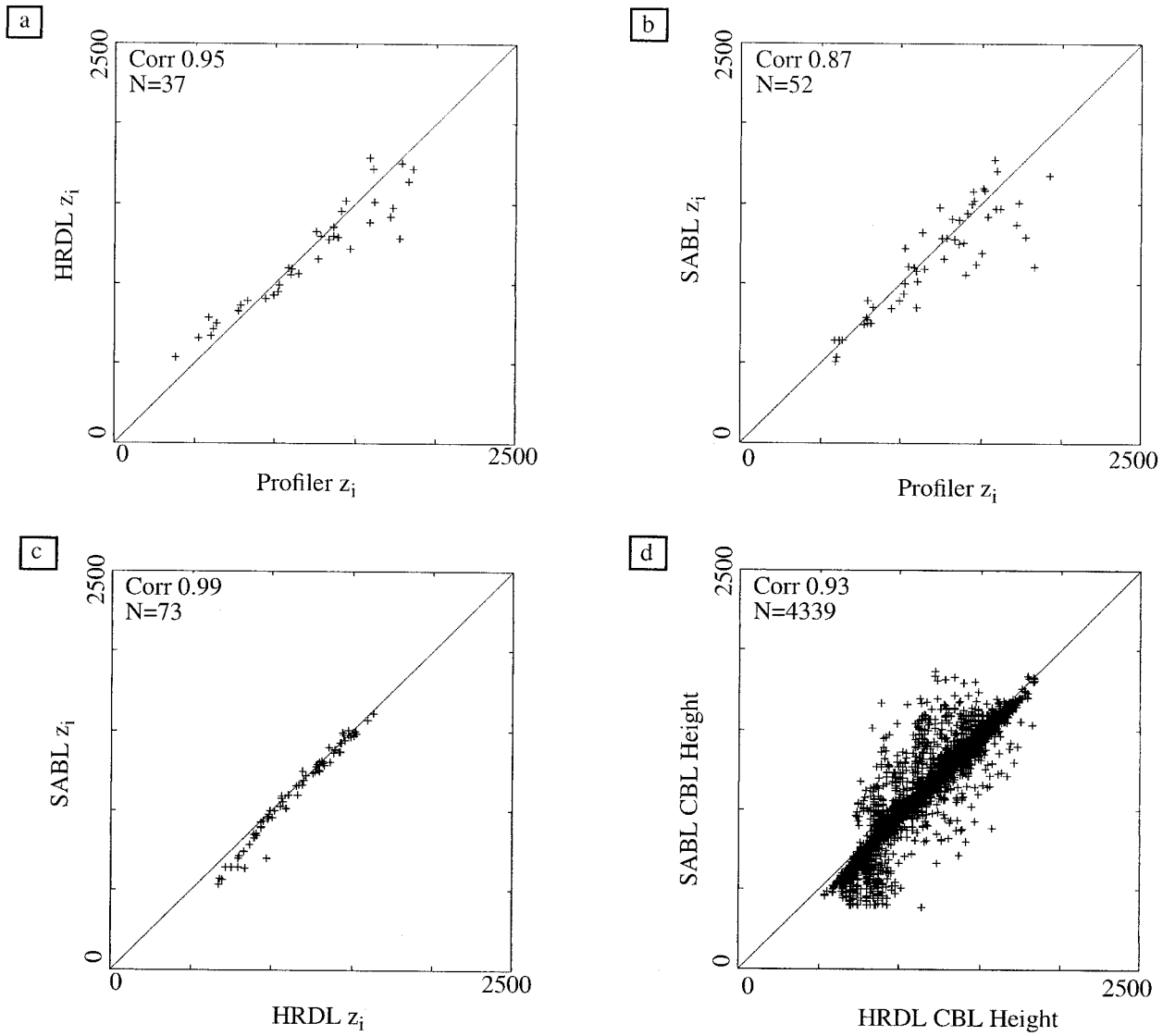

FIG. 5. Comparison of hourly z_i from (a) the wind profiler and HRDL, (b) the wind profiler and SABL, and (c) HRDL and SABL for all available measurements during LIFT. Also (d) comparison of 30-s local CBL top measurements with HRDL and SABL. The 1:1 line is overplotted, and the correlation coefficient and number of points available for comparison also are listed.

The comparison between lidars (Fig. 7c) is relatively good, with a correlation coefficient of 0.80. Comparisons between the wind profiler and each lidar (Fig. 7a and 7b) are less good. We are able to improve the correlations by requiring the measured z_i to differ by even less than one standard deviation, but find that this requirement preferentially excludes points from the afternoon. The best-fit lines show a bias toward a thicker EZ measured by the wind profiler in spite of the closer percentiles used in the profiler calculation. We examined the 30-s measurements of CBL top closely and found that the wind profiler time series shows less coherence from point to point than does the lidar time series. This fact leads the profiler Δz_{ez} to be both larger and less precise than the lidar Δz_{ez}, resulting in the lower correlation. The reason for this larger point-to-point difference is not known.

6. Discussion

There are a number of uncertainties in the z_i estimates shown here. Below we discuss the effect of backscatter from clouds rather than aerosols, effects caused by a profile of aerosol concentration that deviates from the ideal of Fig. 2a, and discuss the residual layer.

a. Effect of clouds

When the lidar pulse encounters an optically opaque cloud, a large amount of backscattered light returns to

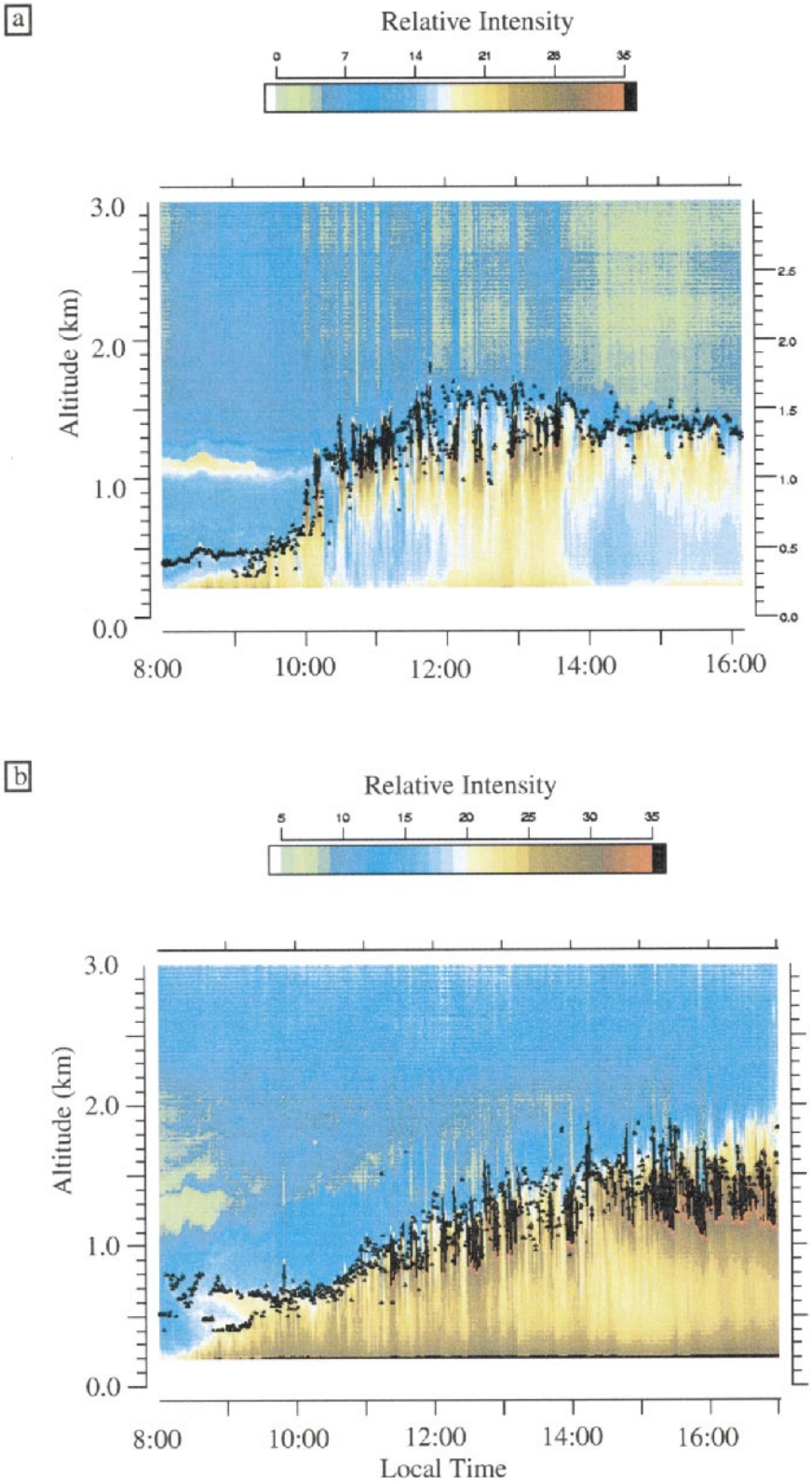

FIG. 6. (a) Measurements of local CBL height (triangles) with SABL for 8 h on 13 Aug 1996 overplotted on backscatter strength. (b) Similar data for 19 Aug 1996. Both examples show complex layering in backscatter in the early-morning boundary layer.

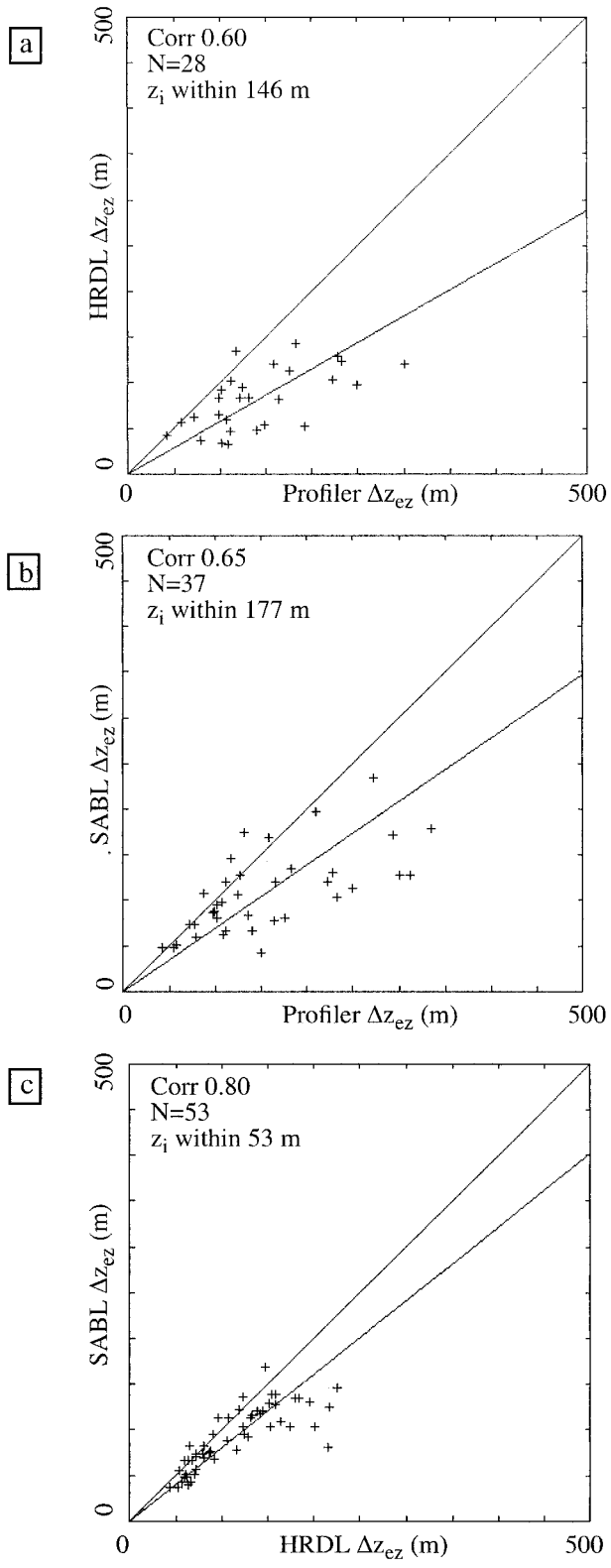

FIG. 7. Comparison of hourly entrainment zone depth from (a) the wind profiler and HRDL, (b) the wind profiler and SABL, and (c) HRDL and SABL. The 1:1 line and best fit (forced through 0) also are plotted. The correlation coefficient, number of estimates, and required agreement in z_i also are listed. See text for description of the estimation technique.

the receiver from the cloud height and none from above it. This effect is visible, for example, in Fig. 1a. In many cases, this effect will result in the backscattered light from the cloud saturating the receiver. In successive range gates, a signal decreasing with range is recorded as the receiver recovers. Although this signature is not related to the atmosphere, it does have a signature similar to the CBL top, that is, a vertical gradient from high to low values, and the wavelet algorithm gives a result slightly above the cloud height. Figure 8a shows an example of a cloud return from HRDL. Because this cloud signal is extremely strong, any averaged profile that includes a cloud return will be dominated by it. An average over 1 h has a high likelihood of encountering cloud, which argues for short averaging times. It also may be possible to separate profiles that include cloud from other data before averaging. Davis et al. (2000) have demonstrated using the largest negative Haar wavelet coefficients to identify a cloud boundary. Identification of clouds is useful information. The relationship of clouds to the entrainment zone and z_i is largely a matter of definition and convention and is especially problematic with moderate cloud fractions. Grimsdell and Angevine (1998) show the relationship between profiler measurements of z_i and cloud-base measurements from a laser ceilometer and discuss the fact that many cloud hits by a lidar or ceilometer are not from cloud base at all but from the sides of clouds tilted by wind shear. We have not specifically attempted to identify clouds using the wavelet algorithm and do not believe they significantly bias our comparison of z_i. The Δz_{ez} calculation is more sensitive to small errors, however, and this effect may be partly responsible for the scatter between lidar and profiler measurements.

b. Effect of a sloped background

Another potential source of bias with the wavelet algorithm is the presence of a sloped aerosol backscatter level within the CBL or free atmosphere. This slope could be due to a variable aerosol concentration or to variations in humidity for aerosols that are hydrophilic. For many days of LIFT, the HRDL lidar inadvertently introduced a sloped background within the CBL. It is possible to set a ''focus'' distance for this lidar at which it will be most sensitive. Although this setting was not recorded, it generally was set low for early-morning measurements and near the expected maximum CBL height during the day. On some days it was set much lower than the top of the CBL, resulting in profiles like that shown in Fig. 8b. At this time it is likely the focus distance was set near 700 m, producing a peak at this range and less sensitivity beyond. Whatever the reason for a sloped background, the Haar wavelet result may be biased to higher (lower) values by a decreasing (increasing) scatter amount with height in the free atmosphere or by an increasing (decreasing) scatter amount with height in the CBL. This bias is illustrated in Figs.

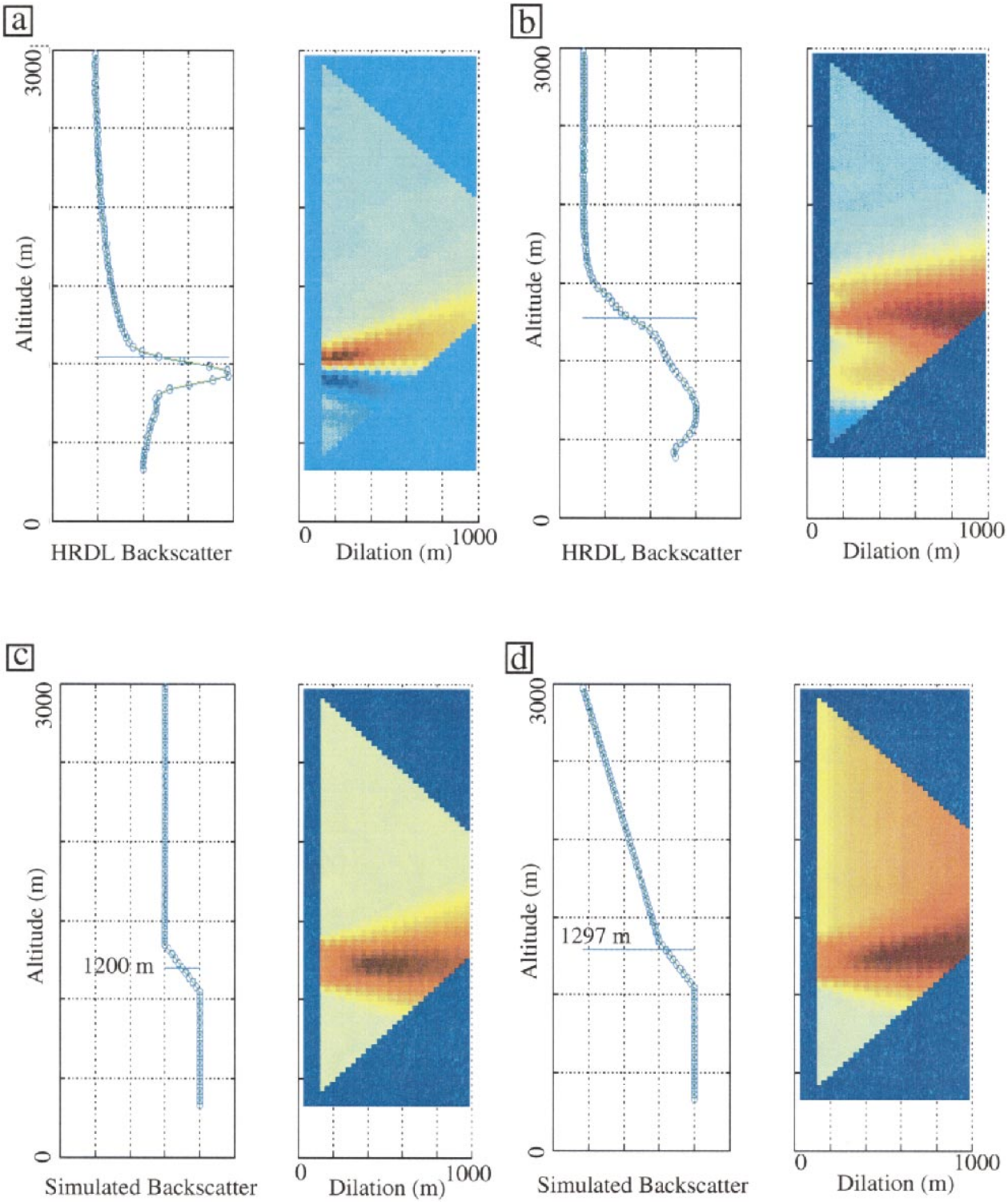

FIG. 8. Examples of lidar backscatter profiles and corresponding wavelet coefficient matrices. (a) Backscatter from a cloud saturating the receiver, (b) example of a sloped backscatter profile in the BL from HRDL, and (c) a simulated ideal backscatter profile and its transform, in comparison with (d) a simulated sloped backscatter profile.

8c and 8d in which a typical profile with entrainment zone centered at 1200 m is shown. When a sloped background is introduced, the algorithm produces a result nearly 100 m too high. Biases such as this one could be responsible for the slight positive bias in HRDL z_i in the mornings.

c. Residual layers

After the afternoon collapse of the CBL, the atmosphere may have a residual layer of air containing properties of BL air (high aerosol concentration) but separated from the true BL by a lower inversion. This case often is true at night, and sometimes a residual layer from the previous day will persist until the next day's CBL grows into it. In Fig. 1c it is seen that the strong convective thermals end at about 1600 LT, and in Figs. 1a and 1b this time is when the small cumulus clouds disappear. The backscatter still shows the residual layer well beyond this time, however. Also, in the early part of this day, the previous day's residual layer is still visible to SABL. The wavelet algorithm may recognize the upper boundary of a residual layer as the top of the CBL because it represents a decrease in backscatter. Our current processing lacks the sophistication to differentiate between layers of decreasing backscatter, so we instead have limited the altitude range searched for a CBL top to eliminate residual layers. Figures 4 and 6 also show examples of residual layers. In Fig. 4, the CBL had likely collapsed by 6 P.M. (1800 LT), but the lidars continue to observe and report an aerosol layer near 1.5 km. On this day, the wind profiler also continues to find a peak in reflectivity at the top of this layer. In Fig. 6, multiple layers in the early morning are seen. When the BL top is too low for the wavelet algorithm to measure it (with a minimum dilation of about 100 m, the BL top must be at least 100 m above the lidar minimum range), a higher layer often will be chosen.

By excluding data from before 1000 and after 1700 LT, we eliminate most residual layer bias from our comparisons. Wavelet algorithms are capable of detecting multiple layers, and continuity or image processing may be used to recognize features such as this one and also other outliers. A fuzzy (continuous) logic approach to this kind of signal processing has shown promise in other geophysical remote sensing areas (e.g., Cornman et al. 1998).

7. Conclusions

We compared measurements of z_i and Δz_{ez} made with lidars and a wind profiling radar over many days during Flatland96 LIFT and found good agreement in z_i and only partial agreement in Δz_{ez}. The agreement in z_i is encouraging, given the very different nature of backscatter mechanisms from lidar and profilers, showing that either kind of instrument can be used to measure z_i routinely. The very good agreement of z_i measured with the two lidars (a correlation of 0.99 for 1-h measurements) is expected and suggests that both instruments are well suited to measuring z_i in boundary layer field experiments. Of course, other characteristics such as the Doppler capability of HRDL or the dual-wavelength capability of SABL differentiate these two instruments. We also have demonstrated a continuous wavelet transform technique for automatically identifying the CBL height in lidar backscatter profiles—a concept previously applied by Davis et al. (1997) and refined by Davis et al. (2000). The wavelet technique has the advantage of allowing us to limit analysis to a chosen range of scales, so that small gradients (e.g., caused by noise) do not interfere with the measurement. Because of this implicit smoothing, the technique does not require averaging of the signals over many minutes to define the feature better. In fact, we are able to use this algorithm at 1-s integration, and similar methods have proven to be useful for airborne lidar measurements. Further work is needed to remove outliers, to identify multiple layers such as residual layers [Davis et al. (2000) have shown a method to find multiple layers but not to identify them robustly as, e.g., the CBL top or a residual layer], and properly to analyze profiles that contain clouds.

Measurements of the entrainment zone thickness with lidars and the wind profiler show considerable scatter, with a correlation of about 0.6. The HRDL and SABL lidars show more consistency (a correlation of 0.8), and airborne lidar measurements presented in Davis et al. (1997) show temporal consistency, although it would be desirable to have an independent measurement for comparison.

The Haar wavelet dilation provides little information on the vertical scale of the gradient in backscatter. Future work will examine backscatter profiles using wavelets other than the Haar to seek a more stable measurement of Δz_{ez}. Also, a wavelet technique will be applied to wind profiler z_i measurements, possibly using a Coif wavelet, which is appropriate for recognizing a local maximum in SNR.

Acknowledgments. We appreciate discussions with C. Holloway, K. Laursen, and B. Morley at the onset of this analysis and acknowledge the efforts of the NCAR and NOAA personnel involved in the LIFT and Flatland96 experiments, especially coinvestigators S. Mayor and C. Grund. K. Davis and one anonymous reviewer also provided comments that greatly improved this paper. Funding for LIFT was provided by the NCAR Atmospheric Technology Division and the NOAA Environmental Technology Laboratory. NCAR is operated by the University Corporation for Atmospheric Research under sponsorship of the National Science Foundation. Flatland96 was supported by NSF under Grant ATM-9419638. This analysis was supported in part by DOE/ARM Grant DEAI05-90ER61070.

REFERENCES

Angevine, W. M., 1999: Entrainment results with advection and case studies from the Flatland boundary layer experiments. *J. Geophys. Res.,* **104,** 30 947–30 963.

——, A. B. White, and S. K. Avery, 1994: Boundary-layer depth and entrainment zone characterization with a boundary-layer profiler. *Bound.-Layer Meteor.,* **68,** 375–385.

——, A. W. Grimsdell, S. A. McKeen, and J. M. Warnock, 1998a: Entrainment results from the Flatland boundary layer experiments. *J. Geophys. Res.,* **103,** 13 689–13 702.

——, A. W. Grimsdell, J. M. Warnock, W. L. Clark, and A. C. Delany, 1998b: The Flatland boundary layer experiments. *Bull. Amer. Meteor. Soc.,* **79,** 419–431.

Boers, R., and E. W. Eloranta, 1986: Lidar measurements of the atmospheric entrainment zone and the potential temperature jump across the top of the mixed layer. *Bound.-Layer Meteor.,* **34,** 357–375.

——, ——, and R. L. Coulter, 1984: Lidar observations of mixed layer dynamics: Tests of parameterized entrainment models of mixed layer growth rate. *J. Climate Appl. Meteor.,* **23,** 247–266.

Carter, D. A., K. S. Gage, W. L. Ecklund, W. M. Angevine, P. E. Johnston, A. C. Riddle, J. Wilson, and C. R. Williams, 1995: Developments in UHF lower tropospheric wind profiling at NOAA's Aeronomy Laboratory. *Radio Sci.,* **30,** 977–1001.

Chui, C. K., 1992: *An Introduction to Wavelets.* Academic Press, 267 pp.

Cohn, S. A., S. D. Mayor, C. J. Grund, T. M. Weckwerth, and C. Senff, 1998: The Lidars in Flat Terrain (LIFT) experiment. *Bull. Amer. Meteor. Soc.,* **79,** 1329–1343.

Cornman, L. B., R. K. Goodrich, C. S. Morse, and W. L. Ecklund, 1998: A fuzzy logic method for improved moment estimation from Doppler spectra. *J. Atmos. Oceanic Technol.,* **15,** 1287–1305.

Crum, T. D., and R. B. Stull, 1987: Field measurements of the amount of surface layer air versus height in the entrainment zone. *J. Atmos. Sci.,* **44,** 2743–2753.

Davis, K. J., D. H. Lenschow, S. P. Oncley, C. Kiemle, G. Ehret, and A. Giez, 1997: Role of entrainment in surface–atmosphere interactions over the boreal forest. *J. Geophys. Res.,* **102,** 29 219–29 230.

——, N. Gamage, C. R. Hagelberg, C. Kiemle, D. H. Lenschow, and P. P. Sullivan, 2000: An objective method for deriving atmospheric structure from airborne lidar observations. *J. Atmos. Oceanic Technol.,* in press.

Driedonks, A. G. M., and H. Tennekes, 1984: Entrainment effects in the well-mixed atmospheric boundary layer. *Bound.-Layer Meteor.,* **30,** 75–105.

Eloranta, E. W., and E. K. Forrest, 1992: Volume-imaging lidar observations of the convective structure surrounding the flight path of a flux-measuring aircraft. *J. Geophys. Res.,* **97,** 18 383–18 393.

Foufoula-Georgiou, E., and E. Kumar, Eds., 1994: *Wavelets in Geophysics.* Academic Press, 373 pp.

Gamage, N., and C. Hagelberg, 1993: Detection and analysis of microfronts and associated coherent events using localized transforms. *J. Atmos. Sci.,* **50,** 750–756.

Grimsdell, A. W., and W. M. Angevine, 1998: Convective boundary layer height measured with wind profilers and compared to cloud base. *J. Atmos. Oceanic Technol.,* **15,** 1331–1338.

Grund, C. J., 1996: High resolution Doppler lidar employing a diode pumped injection-seeded Tm:Lu, YAG transmitter. *Advanced Solid-State Lasers,* S. Payne and C. Pollack, Eds., Optical Society of America, 204–206.

Melfi, S. H., J. D. Spinhirne, S.-H. Chou, and S. P. Palm, 1985: Lidar observation of vertically organized convection in the planetary boundary layer over the ocean. *J. Climate Appl. Meteor.,* **24,** 806–821.

Morley, B. M., K. K. Laursen, L. F. Radke, and A. D. Clarke, 1996: Early results from the Aerosol Characterization Experiment I using airborne lidar and in situ aerosol sampling. *Proc. Second Int. Airborne Remote Sensing Conf. and Exhibition: Technology, Measurements, and Analysis,* Vol. I, San Francisco, CA, Environmental Research Institute of Michigan, 40–48.

Parsons, D., and Coauthors, 1994: The Integrated Sounding System: Description and preliminary observations from TOGA COARE. *Bull. Amer. Meteor. Soc.,* **75,** 553–567.

Piironen, A. K., and E. W. Eloranta, 1995: Convective boundary layer mean depths and cloud geometrical properties obtained from volume imaging lidar data. *J. Geophys. Res.,* **100,** 25 569–25 576.

Rogers, R. R., and M. K. Yau, 1996: *A Short Course in Cloud Physics*. Butterworth–Heinemann Press, 290 pp.

Russell, L. M., D. H. Lenschow, K. K. Laursen, P. B. Krummel, S. T. Siems, A. R. Bandy, D. C. Thornton, and T. S. Bates, 1998: Bidirectional mixing in an ACE 1 marine boundary layer overlain by a second turbulent layer. *J. Geophys. Res.,* **103,** 16 411–16 432.

Steyn, D. G., M. Baldi, and R. M. Hoff, 1999: The detection of mixed layer depth and entrainment zone thickness from lidar backscatter profiles. *J. Atmos. Oceanic Technol.,* **16,** 953–959.

Stull, R. B., 1988: *An Introduction to Boundary Layer Meteorology*. Kluwer, 666 pp.

Walter, G. G., 1994: *Wavelets and Other Orthogonal Systems with Applications.* CRC Press, 245 pp.

White, A. B., C. J. Senff, and R. M. Banta, 1999: A comparison of mixing depths observed by ground-based wind profilers and an airborne lidar. *J. Atmos. Oceanic Technol.,* **16,** 584–590.